Droplet helical motion on twisted fibers

J. Van Hulle[‡], C. Delforge[‡], M. Leonard, E. Follet, and N. Vandewalle[*]
GRASP, Institute of Physics B5a, University of Liège, B4000 Liège, Belgium.

We investigate herein the impact of helical structures on the motion of asymmetrical droplets along vertical twisted fibers. The droplet adopts a helical motion around the bundle, driven by gravity. This complex motion can be manipulated by varying the twist turns of the fibers. When the droplet size is smaller than the characteristic length of the helix (pitch), the droplet adopts a predominant helical motion correlated with the groove of the twisted fibers. When the droplet size exceeds the pitch length, a mixed motion of intermittent vertical sliding and helical movement emerges. A model describes rotational and linear speeds as a function of the fiber twist turns number. This research highlights the profound role of substructures in droplet dynamics, offering fresh insight into droplet manipulation or fiber based devices.

I. INTRODUCTION

Access to water in arid or semi-arid regions remains a critical concern [1]. Extensive research has been conducted on fog harvesting structures to address this challenge. Notable examples include vertical arrays of fibers forming nets or harps [2–4], as well as cut surfaces known as kirigami structures [5, 6]. These innovative designs have demonstrated impressive efficiency in collecting fog droplets. Consequently, understanding the fundamental dynamics of droplets traveling along fibers is a significant area of study. Numerous investigations have focused on manipulating droplets using cylindrical fibers, taking into account factors such as fiber inclination [7–9], intersections [10] and spacing [11, 12] to create guided paths for droplet transport. While the static [13, 14] and dynamic [8] behavior of droplets on cylindrical fibers has been extensively examined, less attention has been given to the substructures of the fibers themselves. A recent article by Leonard *et al.* highlighted the significant influence of these substructures on droplet drainage [15]. Their study revealed that a bundle of two fibers exhibits a convex groove that increases droplet speed by up to 20%. Those convex grooves are also known to enhance the spreading of a droplet inside a one-dimensional horizontal channel [16]. These findings shed light on the importance of exploring droplet dynamics on microstructured substrates.

In the present study, our focus lies on investigating the behavior of droplets traveling down twisted fibers. The torsion of a bundle of two fibers creates a helical structure with a convex groove along the vertical bundle. We thereby create a system with a macrostructure, the vertical fibers, to guide vertically the droplet along with a microstructure, the helical convex groove. We aim to study the influence of this substructure on the motion of asymmetrical-shaped droplets, commonly referred to as clamshell shape, illustrated in Fig. 1.

Our investigation intersects with the recent research conducted by Kern and Carlson [17], which similarly examines the behavior of droplets along two twisted fibers. Their findings reveal distinct droplet trajectories, unveiling significant implications for droplet control and collection applications. It is important to note that our study operates within different experimental conditions. Furthermore, our contribution complements their work by delving deeper into the nuanced dynamics of these particular droplet trajectories. The differences and similarities are explained and highlighted throughout the article.

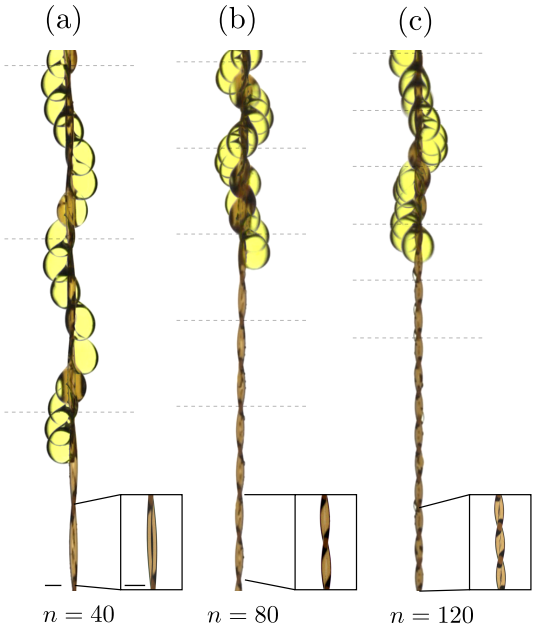

FIG. 1. Superposition of successive pictures of an asymmetrically shaped droplet traveling down on twisted fibers with a helical motion. From left to right, the number of fiber twists increases, $n = 40,\ 80,\ 120$. The dashed horizontal lines represent the fiber pitch. For small n, the droplet follows exactly the substructure, displaying a helical motion, see (a). However, at a larger number of twist values, the droplet exhibits reduced adherence to the tight substructure, resulting in an additional vertical motion, see (b) and (c). The motion is a mix of translations and rotations but the helical motion is no longer correlated with the helical groove of the twisted fibers. The time interval between consecutive pictures is constant at $\Delta t = 0.2$ s. The volume of the droplet is 5 μl and the diameter of one fiber is 0.25 mm. The scale bars on picture (a) correspond to 1 mm.

II. EXPERIMENTAL SECTION

We use nylon fibers (fishing thread) with a fixed diameter, $d = 0.25$ mm. To achieve the desired stretching and twisting of the fibers, a single fiber is threaded through a buckle and fixed at the top on a manual rotation stage. By rotating the screw, both parts of the bundle can be twisted effectively. This helical structure is classified as a twisted double helix [18, 19]. The vertical length of the bundle is fixed at $L = 40$ cm. Each rotation of the screw corresponds to one twist turn of the fibers, denoted as n. A schematic representation of all defined lengths is presented in Fig. 2. The number of twists is given by

$$n = \frac{L}{2\pi b} \tag{1}$$

where $2\pi b$ is the pitch of the helical pattern, with b the reduced helix pitch. Note that twisting of the fibers creates a helical convex groove along the entire bundle. We conducted experiments with up to $n = 200$ twists. As the number of twists increases, so does the tension in the fibers, creating a highly compact structure. However, at higher twist counts, there is a risk of fiber deformation, which can result in non-uniform bundles, or in fiber breaking.

When a droplet adheres to a vertical fiber, it can adopt two distinct configurations: a barrel shape, where the droplet symmetrically engulfs the fiber, or a clamshell shape, where the droplet rests on one side of the fiber, creating an asymmetrical shape [20, 21]. Previous work by Gabbard *et al.* showed that a liquid film descending along a vertical fiber may undergo a destabilization process, resulting in a train of beads exhibiting either a symmetrical (barrel shape) or an asymmetric morphology (clamshell shape) [22]. The occurrence of these configurations depends on factors such as fiber diameter and droplet surface tension. Specifically, the study showed that the asymmetric configuration consistently arises for surface tensions exceeding 50 mN/m. The liquid we choose to use is glycerol with a surface tension of $\gamma \simeq 55$ mN/m. The clamshell shape is therefore the more stable droplet configuration. The density of glycerol is $\rho = 1190$ kg/m^3. We have noticed an important sensibility of the glycerol with temperature. As reported in the literature, the viscosity can decrease by half with an increase of 10°C [23]. Unfortunately, our lab equipment does not allow for precise control on the ambient lab temperature. Furthermore, glycerol

manipulations is also suspected to warm the solution. Nonetheless, we measured a dynamic viscosity of $\eta \simeq 1.2$ Pa.s at around 18°C, and $\eta \simeq 0.8$ Pa.s at around 25°C. The difference factor is about 1.5. The volume of the droplet is fixed at $\Omega = 5$ μl. The droplet is gently deposited on the bundle thanks to an electronic pipette (Eppendorf Xplorer plus). Before each experiment, the bundle is prewetted with several droplets to coat the grooves. For the initialization, at small twist number, 10 droplets are deposited to ensure complete prewetting of the fibers. This prewetting procedure ensures the studied droplets keep a conserved volume. Subsequently, 5 droplets are measured. As the twist turn is increased, 2 prewetting droplets are deposited before the measurement of the subsequent 5 droplets. The contact length of the glycerol droplet on the fibers is constant and is measured, $l = 2.64$ mm. One can also approximate this length with the diameter of a spherical droplet, we have $l \simeq 2\,(3\Omega/4\pi)^{1/3} = 2.1$ mm. The length between the center of the bundle of fibers and the center of the droplet is labeled a and is measured, $a = 0.76$ mm. This length is measured to be constant in all our experiments, the capillary force F_γ that acts at the surface of the droplet overcomes eventual deformations in the droplet shape due to centrifugal forces F_{cf}, the ratio of both forces is estimated $F_{cf}/F_\gamma \sim \rho\Omega\dot{\phi}^2 a/4\pi\gamma\Omega^{2/3} \simeq 0.6$.

In front of the fibers, a CCD camera (Coupled-Charge Device) is positioned to record the droplet motion. The camera captures a portion of the bundle $L_w = 8$ cm. This field of view is 15 cm under the release point of the droplet. A white lighting source is placed behind the fibers to ensure a good contrast of the droplet, and the glycerol is slightly dyed with yellow food coloring. An original Python code is employed to track the linearly increasing position of the droplet over time and to extract the slope to study the linear speed $\dot{z}$. Additionally, as the droplet is traveling around the bundle, one can also count the number of turns of the droplet. The number of turns made by the droplet is denoted τ_w. Consequently, one extracts the angular speed of the droplet $\dot{\phi}$.

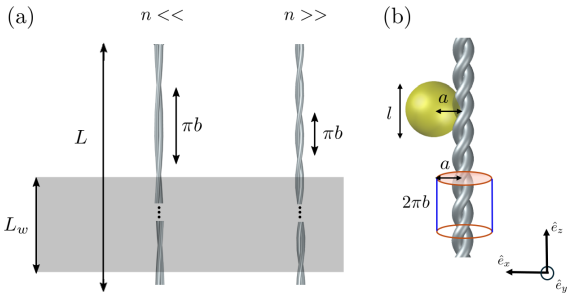

FIG. 2. (a) Sketch of the twisted fibers. We define several lengths, L is the total bundle length, L_w is the portion of the twisted fibers captured by the camera. An increase in the number of turns n leads to a reduction in the half-pitch πb of the helical pattern. (b) Sketch of a spherical droplet on twisted fibers. The distance between the droplet center and the bundle center is labeled a. The length of the droplet is noted l. When the droplet performs a helical motion around the bundle axis with a $2\pi b$ pitch length, the droplet center describes a helix with a radius a which is comprised in a cylinder of radius a and height $2\pi b$.

To reveal key physical parameters, several nondimensional quantities are calculated. The Bond number defined as $\mathrm{Bo} = \rho g\Omega/\gamma l$, compares gravitational and capillary effects. In our experiment, we have a Bo value of around 0.5, indicating that the droplet dynamic is led by both gravitational and capillary effects, such conditions are similar to [15]. The Capillary number estimates viscous effects to surface tension ones, $\mathrm{Ca} = \dot{z}\nu\rho/\gamma$. One obtains values in the range 0.1 to 0.5 with the typical speed values $\dot{z}$ in our experiments. Surface tension overcomes viscous dissipation, allowing the descent of droplets along the fibers. The Weber number compares inertial and surface tension effects, $\mathrm{We} = \rho\dot{z}^2 l/\gamma$, yielding a We number smaller than 0.03, signifying a negligible role of inertia in the present study.

In this experimental setup lies two significant differences with the experiment conducted by Kern and Carlson [17]: the choice of liquid and the prewetting of the fibers. Their research centered on silicone oil droplets, a low

surface tension liquid ($\gamma \simeq 20$ mN/m), descending along dry twisted fibers. In our experiment, prewetting the fibers not only conserves droplet volume but also improves drainage efficiency. These divergent experimental approaches lead to complementary investigations, that expand the understanding of droplet dynamics on twisted fibers.

III. RESULTS AND DISCUSSION

The descending motion of the asymmetrical droplet is significantly influenced by the substructure created by the twist, as shown in Fig. 1. Indeed, the droplet exhibits a helicoidal motion along the twisted fibers. We observe that when the twist turns, denoted n, is small, the droplet follows exactly the twist of the fibers (Fig. 1 (a)). More precisely, one observes the droplet to follow the convex groove. This motion is labeled groove flow by [17]. However, as the number of twist turns increases, the droplet exhibits a combination of helical and vertical motions, as depicted in Fig. 1 (c), labeled as skipping flow [17]. Notably, the distance for one complete turn of the droplet is not correlated with the helical pitch of the twisted fibers. In our experiments, we discern instances where the droplet alternates between rotational and translation motion along several fiber pitches. In Fig. 1 (c), one shows that, at the end of the superposition, the droplet undergoes a vertical descent.

To describe this transition between both dynamical regimes, we measure the number of turns made by the droplet, τ_w. The count is done along the length L_w captured by the camera. We subsequently normalize it to the total length, resulting in

$$\tau = \left(\frac{L}{L_w}\right)\tau_w \tag{2}$$

In Fig. 3, we plot τ as a function of the number of twist turns n. For small values of n, the rotation of the droplet increases linearly with n, this is regime I (groove flow). As n surpasses approximately 80, marking the transition to a second regime, regime II (skipping flow), the number of turns made by the droplet falls to a smaller value that decreases with n.

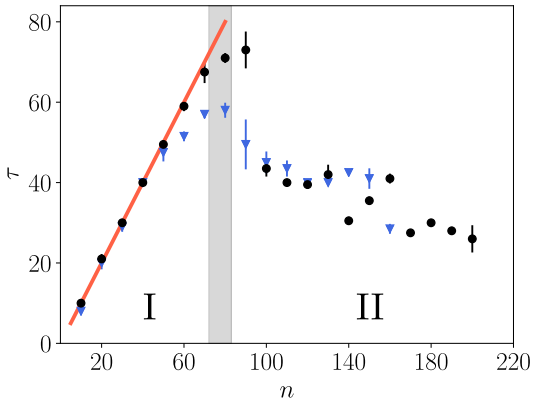

FIG. 3. Number of droplet turns τ as function of fibers twist turns n. Data with black circles (●) are for a low viscosity, around 0.8 Pa.s, and data with blue triangle (▼) are for a higher viscosity, around 1.2 Pa.s. One observes two distinct regimes. In regime I, for $n < 76$, the droplet follows the helical pattern. The number of turns made by the droplet is directly correlated with the fiber twists. The red line is a line of slope 1, i.e. $\tau = n$. In regime II, $n > 76$, the droplet is not following the substructure anymore. The number of turns made by the droplet is a constant. The gray region depicts the transition between both regimes.

We assume that the transition to regime II is linked with the portion of the fiber that the droplet covers. Indeed, as can be seen in Fig. 4, for small values of n, the droplet length l is smaller than the half-pitch of the helical pattern πb (Fig. 4 (a)). On the other hand, for larger n values, the droplet spans several pitches, $l > \pi b$ (Fig. 4 (c)). When the length of the droplet equals the half-pitch, a transition occurs (Fig. 4 (b)). To quantitatively describe this transition, one introduces dimensionless parameter α, which is the ratio between the length of the droplet and the half-pitch [17],

$$\alpha = \frac{l}{\pi b} = \frac{2nl}{L}. \tag{3}$$

At the transition, we assume that $\alpha = 1$. We can thus theoretically approximate the number of twists needed to induce the transition $n_{tr} = 76$. This transition value is well estimated, as can be observed in Fig. 3. The theoretical transition is described in each plot with a vertical gray range. The width of this range is calculated by considering the error made on the droplet length l, we have $l = 2.64 \pm 0.16$ mm.

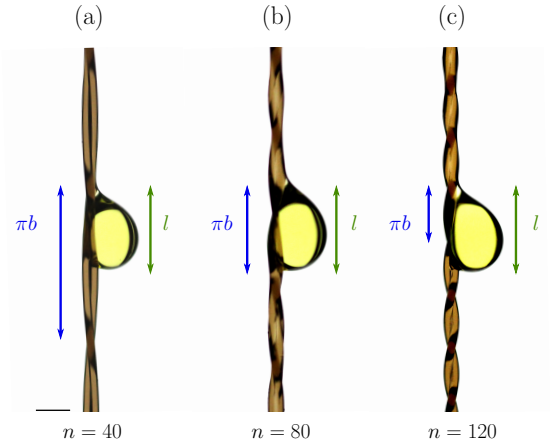

FIG. 4. Pictures of a droplet on several twisted fibers. From left to right, the number of fiber twists increases, $n = 40,\ 80,\ 120$. This emphasizes the covered length of the droplet l on the twisted fibers (green), a key parameter to distinguish the motions adopted by the droplet. The half-pitch of the helical pattern created by the twisted fibers is depicted in blue. (a) The droplet's length is shorter than half the pitch. Under such conditions, the droplet exhibits a purely helical motion. (b) The droplet's length is the same as the half-pitch. (c) The droplet's length is longer than the half-pitch, which induces a combined behavior of helical motion and vertical sliding. The volume of the droplet is 5 μl and the diameter of the fiber is 0.25 mm. The scale bar corresponds to 1 mm.

One can examine the droplet dynamics in both regimes. Note that both the angular speed and the vertical speed are constant for a given value of twists n thanks to the prewetting of the bundle. First, in Fig. 5 (a), we plot the angular speed $\dot{\phi}$ of the droplet as a function of α, for two different viscosities of the same mixture at different temperatures. In regime I, the angular speed increases with the twist turns, while in regime II, it decreases. This trend is also observed in [17] for the groove and skipping flows. Next, in Fig. 5 (b), we plot the non-dimensional linear speed $\dot{z}/\dot{z}_{n=0}$, as a function of the dimensionless parameter α (see Eq. (3)). The denominator $\dot{z}_{n=0}$ stands for the linear speed of the droplet on two parallel fibers, this value is obtained thanks to the models developed in the following section. It represents the characteristic descending speed of clamshell shape droplet on a fiber bundle. Interestingly, in regime I ($\alpha < 1$), we observe an important decrease in the linear speed with α while in regime II ($\alpha > 1$), it decreases more slowly with α. Surprisingly, this influence of the twists on the linear speed is not observed when the fibers are not prewetted [17]. In both Fig. 5 (a) and (b), one notices that a change in viscosity does not affect the trend of the data, a decrease in the viscosity only results in an increase of the angular and vertical speeds. In the following subsections, we describe the observed trends thanks to one model for each regime.

A. Models

In the first instance, to differentiate the motions in both regimes, the ratio $\dot{z}/(b\dot{\phi})$ is plotted in Fig. 6 (a). The relation $\dot{z}/(b\dot{\phi}) = 1$ is characteristic of a helical motion. In the first regime, for $\alpha < 1$, this ratio is approximately 1, with a mean value of 0.9. This regime is dependent on the characteristic length of the helix, $2\pi b$. Interestingly, in the second regime, the relationship between vertical and angular speed is not correlated with the helix length. When the droplet size is larger than the half-pitch, it changes the characteristic length. In the second regime, the capillary length of the droplet l_c and the relative size of the droplet compared to the helix, α, are important parameters. This is depicted in Fig. 6 (b) where the ratio $\dot{z}/(\alpha l_c\dot{\phi})$ is plotted. It shows a constant value in the second regime, with a mean value of 0.4. The transition

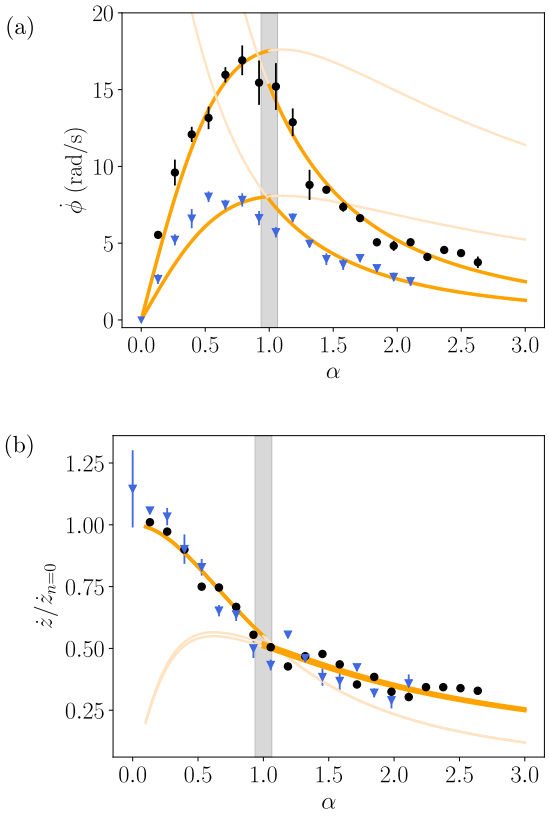

FIG. 5. (a) Angular speed $\dot{\phi}$ as a function of α. In regime I, $\alpha < 1$, the angular speed increases with α. In regime II, $\alpha > 1$, it is slightly decreasing. The colored curves are fit of Eq. (8) and Eq. (10) on the respective regime. (b) Non-dimensionalized linear speed $\dot{z}/\dot{z}_{n=0}$ as a function of α. In regime I, $\alpha < 1$, the non-dimensional linear speed decreases with α. In regime II, $\alpha > 1$, it decreases more gently. The orange curves are fit of Eq. (9) and Eq. (11). Data with black circles (•) are for a low viscosity and data with blue triangles (▼) are for a higher viscosity. The gray region both in (a) and (b) depicts the transition between the two regimes.

between regimes signifies a change in the dominant parameter, the first regime is governed by the helix pitch $2\pi b$ (Fig. 6 (a)), while the second regime is dominated by the capillary length and the relative size of the droplet compared to the half-pitch (Fig. 6 (b)). This transition marks a shift from a regime where the helical structure dictates the motion to one where capillary length controls the descent, combining helical motion with vertical sliding.

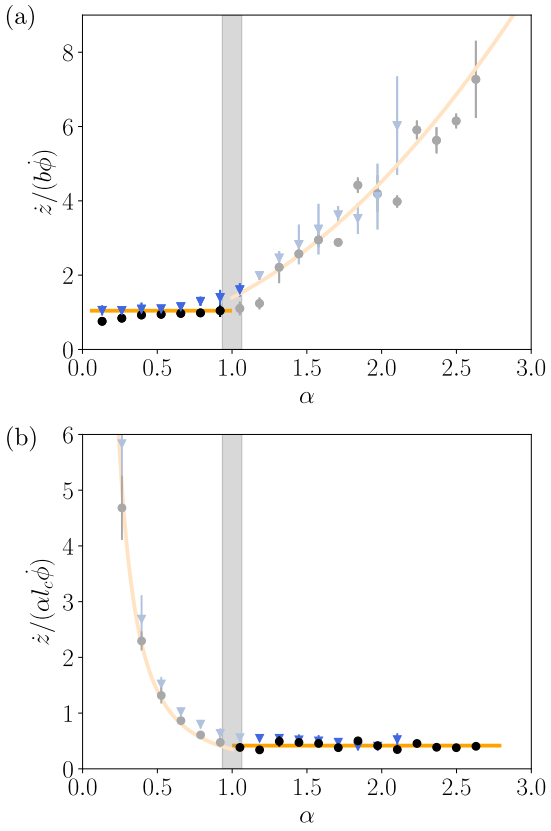

FIG. 6. (a) Ratio $\dot{z}/(b\dot{\phi})$ as a function of α. For $\alpha < 1$, the ratio is constant, with a mean value close to one. The first regime is linked with the characteristic length of the helical groove of the bundle. For $\alpha > 1$, the vertical and the angular speeds relation is not defined by the helix pitch $2\pi b$, showing an increasing trend with α. (b) Ratio $\dot{z}/(\alpha l_c\dot{\phi})$ as a function of α. This ratio is constant in the second regime ($\alpha > 1$), with a mean value of 0.4. This is indicative that the capillary length times the droplet's relative size to the half-pitch is the relevant characteristic length in this regime. One observes no influence of the viscosity.

To describe the particular motion of the droplet, one can notice that the center of mass of the droplet follows a helical path inscribed on the surface of a cylinder. The height of the cylinder is $2\pi b$ and its radius is a, as illustrated in Fig. 2 (b). Two capillary forces act at both ends of the droplet. These capillary forces act as adhesive forces, promoting rotation around the bundle by creating a resultant force directed towards the cylinder's interior. To describe the helical motion of the center of mass, one can unroll the cylinder into a rectangular representation with a length $2\pi a$, corresponding to the perimeter of the cylinder base, and a width $2\pi b$, corresponding to the pitch of the helix, as represented in Fig. 7. This representation also includes the grooves between the fibers, which are parallel to the diagonal of the rectangle. Two grooves are represented, the one in front of the bundle and the one at the rear. Depending on the relative size of the droplet compared to the half-pitch, the droplet may either sit on a single groove ($\alpha < 1$, see Fig. 7 (a)) or span on multiple grooves ($\alpha > 1$, see Fig. 7 (b)).

To model the behavior observed in the different regimes, we use a balanced force model. The droplet motion is driven by its weight, which is balanced by viscous dissipation. Inertia can be neglected due to the Weber number and the constant velocities observed during helical motion at fixed torsion. We therefore consider a balance between the dissipation force and the driving gravitational force along the fiber groove, as sketched in Fig. 7 (a) and (b). The dissipation force is given by

$$F_\eta = \xi \eta l v \tag{4}$$

with ξ a geometrical parameter and v the total speed of the droplet which is given by

$$v = \sqrt{\dot{z}^2 + (a\dot{\phi})^2}. \tag{5}$$

The gravitational component along the groove is given by

$$F_{g,h} = \rho g \Omega \sin(\theta), \tag{6}$$

where θ is the slope of the helix and is given by $\tan\theta = b/a$. This leads to

$$F_{g,h} = \rho g \Omega \frac{b}{\sqrt{b^2 + a^2}}. \tag{7}$$

Balancing both forces allow to describe the observed trend of $\dot{z}$ and $\dot{\phi}$ as explained in the following sections.

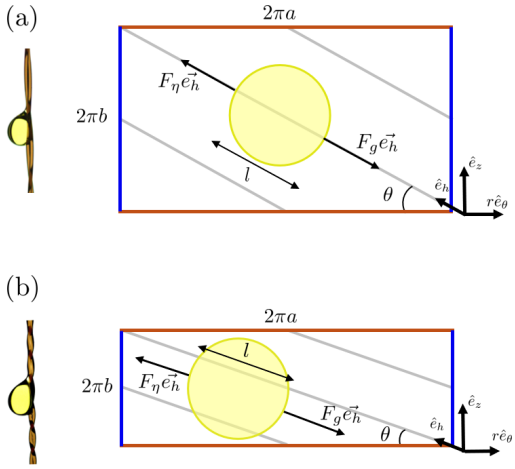

FIG. 7. Representation of the unrolled cylinder on which the helical motion is inscribed. The length is given by the perimeter of the cylinder base, $2\pi a$, and the width by the pitch of the helix, $2\pi b$. The grooves of the fiber bundle are depicted as gray lines parallel to the diagonal of the rectangle. The slope of the helix is labeled θ. In regime I, where the droplet length l is smaller than the half-pitch πb, the droplet sits on one groove, as shown in (a). In regime II, the droplet spans several grooves, as shown in (b). In both cases, the motion is attributed to a balance between the driving gravitational force and the dissipating friction force.

B. Regime I

In this subsection, we model the droplet motion when it adheres to the spiral pattern of the twisted fibers. We assume the motion of the droplet to be a helix with (i) a reduced pitch b_{drop} equal to the reduced pitch of the twisted fibers, $b_{drop} = b$, and with (ii) a radius a given

by the length between the center of the bundle of fibers and the center of the droplet. In the regime I, the relation between the vertical speed and the angular speed is given by $\dot{z} = b\dot{\phi}$ as shown in Fig. 6 (a). Injecting this relation into Eq. (5) and balancing the weight and the dissipation, leads to the expression of the angular speed,

$$\dot{\phi}_I = \frac{\rho g \Omega}{\xi_I \eta l} \frac{b}{b^2 + a^2}. \tag{8}$$

Then, one obtains the vertical speed,

$$\dot{z}_I = b\dot{\phi}_I = \frac{\rho g \Omega}{\xi'_I \eta l} \frac{b^2}{b^2 + a^2}. \tag{9}$$

In these two relations, we have two unknown parameters ξ_I and ξ'_I for dissipation, that are used as fitting parameters. These two coefficients account for the different dissipation in angular motion and vertical motion.

C. Regime II

In this subsection, we describe the motion of a droplet in the second regime where an intermittent vertical sliding are observed. The droplet sometimes adheres to the helical fiber substructure and sometimes slides along the bundle. The ingredients are the same as before except for the relation between the vertical speed and the angular speed. As shown in Fig. 6 (b), one has the following relationship $\dot{z} = \alpha l_c \dot{\phi}$. We obtain the following expressions,

$$\dot{\phi}_{II} = \frac{\rho g \Omega}{\xi_{II} \eta l} \frac{b}{\sqrt{(\alpha l_c)^2 + a^2}\sqrt{b^2 + a^2}}, \tag{10}$$

and

$$\dot{z}_{II} = \alpha l_c \dot{\phi}_{II} = \frac{\rho g \Omega l_c}{\xi'_{II} \eta l} \frac{\alpha b}{\sqrt{(\alpha l_c)^2 + a^2}\sqrt{b^2 + a^2}}, \tag{11}$$

with ξ_{II} and ξ'_{II} two dissipation coefficients for the dissipation in the second regime.

D. Analysis

The previously described models can be adjusted on the experimental data for each regime. We divide the data into both regimes: regime I with $\alpha < 1$ and regime II with $\alpha > 1$, to fit the corresponding model on each regime. In Fig. 5 (a) and Fig. 5 (b), we plot the angular speed and the non-dimensional vertical speed as a function of α, with the orange lines representing the model fittings. The non-dimensional vertical speed is obtained by dividing the vertical speed $\dot{z}$ by the vertical speed of a droplet on parallel fibers $\dot{z}_{n=0}$. The latter is obtained by extrapolating the model to the case of zero twist turns, $n = 0$, which corresponds to an infinite pitch, $2\pi b \to \infty$. The models depict well the observed behaviors. In the model, ξ and ξ' are the fitting parameters. We find that the fitting parameters are of the same order of magnitude across both regimes. The fitting parameters are given in Table I. As the temperature is not well controlled in our laboratory, the error on the fluid viscosity η could influence the value of ξ. One notices that the fitting parameter is systematically larger for the higher viscosity. Although the fitted values are similar, the difference can be attributed to a different dissipation between helical and vertical motions. Specifically, in regime II, the droplet slides along multiple pitches and grooves, which can result in a higher dissipative coefficient for the vertical motion. Indeed, it is known that horizontally oriented fibers intersecting the path of a vertically descending droplet have a significant influence on its behavior [8, 13]. The droplet may either continue its motion or stop, hung on the horizontal fiber. In our case, the droplet moves along a fiber with periodic bumps, due to the substructure, which may act as obstacles along the droplet's path, explaining the different dissipation in the angular and vertical motions in the second regime. Also, the lack of precise temperature control may affect the viscosity and, consequently, the fitting parameters.

	Low viscosity	High viscosity
ξ_I	1.04	1.5
ξ_{II}	0.59	0.76
ξ'_I	1.05	1.1
ξ'_{II}	1.41	1.52

TABLE I. Comparison of the obtained fitting parameters. The fitting values obtained for the angular speed in regimes I and II, ξ_I and ξ_{II} respectively, are compared with the ones for the vertical speed in regimes I and II, ξ'_I and ξ'_{II}, respectively. It is observed that the values are systematically higher for the high viscosity fluid.

IV. CONCLUSIONS

In this paper, we study the helicoidal and translational dynamics exhibited by a droplet traveling along vertical twisted fibers for two different viscosities. The droplet exhibits an asymmetric clamshell shape due to the high surface tension of glycerol. Twisting two cylindrical fibers creates a specific bundle with a helical convex shape groove. This substructure considerably influences the droplet's motion. Indeed, depending on the twist turns, the droplet is seen to adopt a predominantly helical trajectory or a predominantly vertical one. These reveal two regimes that depend on the relative dimensions of the droplet and of the helical pitch, as also observed in [17]. When the droplet size is smaller than the pitch, the droplet has a high tendency of adhering to the helical substructure. Conversely, when the droplet size surpasses the pitch length, then the droplet that spans on several grooves exhibits a mixture of motion composed of vertical sliding and helical motion. Furthermore, we show that increasing the viscosity decreases both speeds but does not affect their trends with the twist turns. We develop a model that describes the experimental data of the rotational speed and the linear speeds. In addition, we observe a larger dissipative coefficient for the vertical motion in the second regime explained by the fact that the droplet encounters several bumps due to the helical structure of the fibers.

This study shed light on the importance of substructures that can change the behavior of the droplet's motion. We achieve the rotation of the droplet along a vertical fiber, thereby opening avenues for three-dimensional manipulation of droplets. It enables the droplet to go from either the right-left or front-back side of the fiber. Additionally, this rotational motion affords the droplet an expanded interaction area with the surrounding gas phase, which holds promise for application in droplet-gas interaction [24, 25]. This experiment is also a creative adaptation of a bead moving along a helical wire, a usual problem taught in classical mechanics. Indeed, the soft matter beads leads to transitional behavior and unusual motions. Finally, this study has potential implications for enhancing droplet drainage of droplets along fibers. Specifically, we highlight that small torsions in a bundle of fibers induce larger vertical speeds than high twisted bundles. Draining efficiency is a key problem in water-harvesting structures, particularly in fiber-based configurations such as harps or nets [3, 4]. This study holds promise for optimizing the performance of such structures in water collection applications. For further insights into practical applications, we highly recommend exploring the paper authored by Kern and Carlson [17], which offers fascinating demonstrations of droplet manipulation and collection on twisted fibers. This study also opens potential avenues for future research on liquid retention on twisted fibers. Performing an experiment of a twisted bundle outward from a liquid bath could be interesting to investigate the thickness and the stability of the prewetting liquid inside the helical convex groove.

ACKNOWLEDGMENTS

This work is financially supported by the University of Liège through the CESAM Research

Unit.

AUTHOR INFORMATION

Corresponding Author

* Email: nvandewalle@uliege.be

Author contributions

C.D., E.F. and J.V.H. conducted all experiments. J.V.H. and C.D. worked together closely on post-processing the experimental data. J.V.H., M.L., and N.V. contributed to the model development. J.V.H. took the lead in writing the article. All authors played integral roles in data analysis and contributed collectively to the article's composition. ‡ J.V.H. and C.D. contributed equally.

NOTE

The authors declare no competing financial interest.

V. REFERENCES

[1] WWAP, *The United Nations World Water Development Report 2023: partnerships and cooperation for water*; UNESCO: Paris, 2023.

[2] Shi, W.; Anderson, M. J.; Tulkoff, J. B.; Kennedy, B. S.; Boreyko, J. B. Fog Harvesting with Harps. *ACS applied materials & interfaces* **2018**, *10*, 11979–11986.

[3] Shi, W.; van der Sloot, T. W.; Hart, B. J.; Kennedy, B. J.; Boreyko, J. B. Harps enable water harvesting under light fog conditions. *Adv. Sust. Syst.* **2020**, *4*, 2000040.

[4] Jiang, Y.; Machado, C.; Park, K. K. From capture to transport: A review of engineered surfaces for fog collection. *Droplet* **2023**, *2*, e55.

[5] Li, J.; Ran, R.; Wang, H. W. Y.; Chen, Y.; Niu, S.; Arratia, P. E.; Yang, S. Aerodynamics-assisted, efficient and scalable kirigami fog collectors. *Nat Commun* **2021**, *12*, 5484.

[6] Bintein, P.-B.; Cornu, A.; Weyer, F.; De Coster, N.; Vandewalle, N.; Terwagne, D. Kirigami fog nets: how strips improve water collection. *npj Clean Water* **2023**, *6*, 54.

[7] Huang, Z.; Liao, X.; Kang, Y.; Yin, G.; Yao, Y. Equilibrium of drops on inclined fibers. *J. Colloid Interface Sci.* **2009**, *330*, 399–403.

[8] Gilet, T.; Terwagne, D.; Vandewalle, N. Droplets sliding on fibres. *Eur. Phys. J. E.* **2010**, *31*, 253–262.

[9] Poulain, S.; Carlson, A. Sliding, vibrating and swinging droplets on an oscillating fibre. *J. Fluid Mech.* **2023**, *967*, A24.

[10] Weyer, F.; Duchesne, A.; Vandewalle, N. Switching behavior of droplets crossing nodes on a fiber network. *Scientific Reports* **2017**, *7*, 13309.

[11] Duprat, C.; Protière, S.; Beebe, A. Y.; Stone, H. A. Wetting of flexible fibre arrays. *Nature* **2012**, *481*, 510–513.

[12] Gabbard, C. T.; Bostwick, J. B. Thin film flow between fibers: Inertial sheets and liquid bridge patterns. *Phys. Rev. Fluids* **2023**, *8*, 110505.

[13] Lorenceau, E.; Clanet, C.; Quéré, D. Capturing drops with a thin fiber. *J. Colloid Interface Sci.* **2004**, *510*, 29–45.

[14] Pan, Z.; Weyer, F.; Pitt, W. G.; Vandewalle, N.; Truscott, T. T. Drop on a Bent Fibre. *Soft Matter* **2018**, *14*, 3724–3729.

[15] Leonard, M.; Van Hulle, J.; Weyer, F.; Terwagne, D.; Vandewalle, N. Droplets sliding on single and multiple vertical fibers. *Phys. Rev. Fluids* **2023**, *8*, 103601.

[16] Van Hulle, J.; Vandewalle, N. Effect of groove curvature on droplet spreading. *Soft Matter* **2023**, *19*, 4669.

[17] Kern, V. R.; Carlson, A. Twisted fibers enable drop flow control and enhance fog capture. *Proceedings of the National Academy of Sciences* **2024**, *121*, e2402252121.

[18] Olsen, K.; Bohr, J. The generic geometry of helices and their close-packed structures. *Theoretical Chemistry Accounts* **2010**, *125*, 207–215.

[19] Hanlan, J. M.; Davis, G. E.; Durian, D. J. Twist and measure: characterizing the effective radius of strings and bundles under twisting contraction. *Soft Matter* **2023**, *19*, 4315–4322.

[20] McHale, G.; Newton, M. I.; Carroll, B. J. The Shape and Stability of Small Liquid Drops on Fibers. *Oil Gas Sci Technol* **2001**, *56*, 47–54.

[21] McHale, G.; Newton, M. I. Global geometry and the equilibium shapes of liquid drops on fibers. *Colloid. Surface.* **2002**, *206*, 79–86.

[22] Gabbard, C. T.; Bostwick, J. B. Asymmetric instability in thin-film flow down a fiber. *Phys. Rev. Fluids* **2021**, *6*, 034005.

[23] Segur, J. B.; Oberstar, H. E. Viscosity of glycerol and its aqueous solutions. *Industrial & Engineering Chemistry* **1951**, *43*, 2117–2120.

[24] Sadeghpour, A.; Zeng, Z.; Ji, H.; Dehdari Ebrahimi, N.; Bertozzi, A. L.; Ju, Y. S. Water vapor capturing using an array of traveling liquid beads for desalination and water treatment. *Sci. Adv.* **2019**, *5*, eaav7662.

[25] Chinju, H.; Uchiyama, K.; Mori, Y. H. "String-of-beads" flow of liquids on vertical wires for gas absorption. *AIChE journal* **2000**, *46*, 937–945.

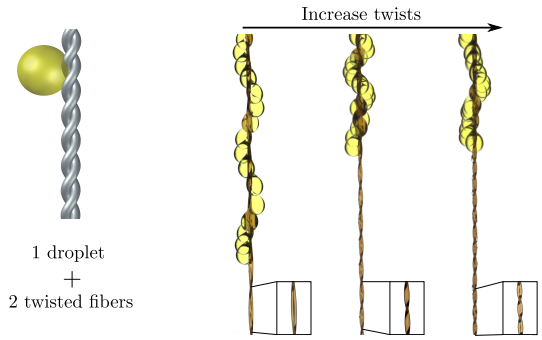

FIG. 8. TOC Graphic